Available online at www.sciencedirect.com
SCIENCE DIRECT®
Dynamics of Atmospheres and Oceans
37 (2004) 295–311
dynamics of atmospheres and oceans
www.elsevier.com/locate/dynatmoce

Evaluation of the ERA-40 air–sea surface heat flux spin-up

S. Ramos Buarque*, H. Giordani, G. Caniaux, S. Planton

Météo-France, CNRM/GMGEC/MEMO, 42 Avenue Gaspard Coriolis, 31057 Toulouse Cedex 1, France

Received 21 May 2002; received in revised form 25 August 2003; accepted 13 October 2003

Abstract

Ocean models depend strongly on surface fluxes. When computed from atmospheric models, fluxes are affected by spin-up, i.e. they increase (or decrease) with forecast length. Such behavior may bias ocean models. The European Centre for Medium Range Forecasts (ECMWF) 40-year re-analysis (ERA-40) has been used to quantify short-range spin-ups of radiative and turbulent heat fluxes. Fluxes are compared as differences between two runs with the same initialization time. This method allows flux analysis over short-range forecasts as a function of distance from the initialization time. Results indicate that (i) latent heat flux spin-up increases with time but levels off after 24 h; (ii) sensible and radiative flux spin-ups remain constant after 6 h; (iii) regional spin-up of turbulent fluxes are systematic and can be larger than 30% for sensible heat but never exceeds 15% for latent heat; (iv) spin-up depends upon the season. The same analysis has been carried out with the ECMWF 15-year re-analysis (ERA-15); spin-ups in ERA-40 have been generally smaller than those in ERA-15.

Keywords: Air–sea surface heat fluxes; Spin-up; Short-range forecast; Re-analysis; ERA-40; ERA-15

1. Introduction

Global Numerical Weather Prediction (NWP) and data assimilation methods developed rapidly during the 1980s due to advances in computer technology. Data assimilation systems were able to merge observations irregularly distributed in time and space and collected on various observational platforms. However, long time series of analyses suffer from inconsistencies due to model changes and continuous improvement of data assimilation schemes. Bengtsson and Shukla (1988) and Trenberth and Olson (1988) proposed reanalyzing past atmospheric data sets by using the best assimilation system available. Their proposals led to three major projects: the 15-year re-analysis (ERA-15) of the European Centre for Medium

* Corresponding author. Tel.: +33-5-61-07-96-51; fax: +33-5-61-07-96-10.
E-mail address: silvana.buarque@cnrm.meteo.fr (S. Ramos Buarque).

0377-0265/$ – see front matter © 2003 Elsevier B.V. All rights reserved.
doi:10.1016/j.dynatmoce.2003.10.001

Range Forecasts (ECMWF) (Gibson et al., 1999); the 50-year analysis of the National Centers for Environmental Prediction (NCEP) (Kistler et al., 2001); and the 15-year analysis of the National Aeronautics and Space Administration (NASA) (Schubert et al., 1993).

From these homogeneous series, several applications were derived: oceanic simulations forced by heat and momentum fluxes, decadal, intraseasonal and interannual variability studies, hydrological cycle studies, etc. These applications provided a great motivation to produce these re-analyses. However, it soon became necessary to re-run longer analyses to take advantage of updated assimilation systems and model improvements. Such ambitions encouraged the ECMWF to run a new 40-year re-analysis (ERA-40) with the most recently available assimilation system (Simmons and Gibson, 2000).

Surface fluxes strongly depend on imbalances between the initial conditions and the atmosphere consistent with the forecast model's physics and dynamics (White and Saha, 1999). This imbalance originates substantial shifts of air–sea surface fluxes during the first time steps over model integration. During this period, model's wind and mass fields are not balanced themselves resulting in unrealistic air–sea surface fluxes. Fluxes obtained during this phase cannot be used to perform budgets even if it is near to observations (Giordani and Planton, 2000). This phase is called spin-up period. In order to overcome this problem, ocean models are generally forced with fluxes averaged from 6 or 12 h forecast rather than the analysis. However, this elapsed time is normally chosen empirically because little information is available on spin-up periods.

In this paper, spin-up evolutions are examined in order to estimate more accurately the period beyond which spin-up problems cease. A second purpose is to compare spin-ups of air–sea surface fluxes of ERA-40 and ERA-15.

2. The ECMWF re-analysis

The ERA-40 project (http://www.ecmwf.int/research/era) covers the period from September 1957 to August 2002. The production was split into four streams: the first priority production period from 1989 to 2002 (Stream 1); the second from October 1957 to end-1972 (Stream 2); the third from 1972 to 1985 (Stream 3) and the last from 1986 to 1989 (Stream 4). The project started in Autumn 2000 and results will be available in Autumn 2003 (Uppala et al., 2000). Some details of the model are given hereafter.

2.1. Model resolution

Table 1 summarizes the configuration of ERA-40 in comparison with ERA-15. ERA-40 has a spectral representation based on a triangular truncation at wave number 156, which corresponds to a Gaussian grid of 1.125° (about 125 km). In the vertical, ERA-40 has 60 hybrid levels with the highest at 0.1 hPa.

2.2. Assimilation technique

The main improvement of ERA-40 compared to ERA-15 concerns the assimilation scheme. ERA-40 uses the three-dimensional variational (3D-Var) technique, while ERA-15

Table 1
Main differences between ERA-40 and ERA-15 assimilation systems

Analyze	ERA-40	ERA-15
Spatial resolution	Spectral T159 resolution with 60 vertical hybrid levels	Spectral T106 resolution with 31 vertical hybrid levels
Assimilation mode	Three-dimensional variational (3D-VAR) analysis with 6 h cycling	Statistical optimum Interpolation (OI) analysis with 6 h cycling
Continuous data	Physical retrieval of satellite radiance data incorporated in 3D-VAR analyses	One-dimensional variational (1D-VAR) analysis of the Cloud-Cleared Radiances (CCR)

used Optimal Interpolation (OI). The OI algorithm performs observation selection by attributing them a weight based on the background error covariance. In practice, the background error covariance is assumed small for large separations, so that only observations in a limited geometrical domain around the model grid point are selected. Spurious noise produced by the OI is filtered by an orthogonal normal mode procedure to get a balanced initial state (Lorenc, 1981).

The essence of the 3D-Var algorithms is to rewrite the least-square problem as the minimization of a cost-function. The method was introduced in order to remove the local data selection of the OI. 3D-Var uses complex observation operators and solves the adjoint equations of the model. The main difficulty of both techniques is to specify the model background error covariance (Courtier et al., 1998).

2.3. Assimilated data

The new variational assimilation techniques of ERA-40 allow direct assimilation of raw radiance from TIROS Operational Vertical Sounder (TOVS) instruments. In ERA-15, data from the TOVS instruments was assimilated in the form of Cloud-Cleared Radiances (CCR), which had already passed through several preprocessing steps. ERA-40 also uses SSM/I passive microwave to analyze the total column water vapor and 10 m wind speed (Kelly and Li, 2002). In ERA-15, sea ice cover was derived from SSM/I following a quality control process that uses reliable Sea Surface Temperatures (SST) analysis (Nomura, 1997). In ERA-40, sea ice cover and SST were taken respectively from Met Office Hadley Centre and 2D-Var NCEP analyses (Rayner et al., 2002). Both re-analysis use Cloud Motion Winds (CMW) from geostationary satellites. More information about observational data can be found at the ECMWF Reanalysis Web site quoted above.

2.4. Air–sea fluxes

In ERA-40 as in ERA-15, parameterization of turbulent fluxes is based on the Monin–Obukhov similarity theory. The transfer coefficients depend on stability functions. However, the parameterization of ERA-40 has been updated (Beljaars, 1995, 1997). In particular, the roughness length for momentum is computed with a Charnock constant estimated from a fully coupled ocean wave model (Janssen et al., 1997). The roughness lengths

for momentum, heat and moisture also include a free convection velocity scale, which represents the near-surface wind induced by eddies in the free-convection regime.

3. Methodology

3.1. Definitions

To evaluate the spin-up, several forecast lengths are needed, which depend on availability of fluxes. ERA-40 and ERA-15 archives follow the forecast lead-time production, i.e. the model run defined by its initialization time and duration. Initialization time is denoted hereafter as [Time] and the run duration as [Step]. With this convention, ERA-40 fluxes are archived with:

$$[\text{Time}] = 0, 12; \quad [\text{Step}] = 0, 3, 6, 12, 18, 24, 30, 36$$

$$[\text{Time}] = 0, 18; \quad [\text{Step}] = 0, 3, 6$$

In ERA-15 the same flux series are available except for $[\text{Step}] = 30,\ 36$ at $[\text{Time}] = 0,\ 12$.

Publications in the open literature (Hagemann et al., 2002; Arpe and Stendel, 1996; Arpe, 1996) evaluate precipitation spin-up trends by examining of forecast lead-times. In this kind of analysis, spin-up signals are smoothed because longer forecast lead-times always include previous information, i.e. global averages for 0–30 h forecast take into account information related to 0–24 h forecast. A second point is that temporal variability of precipitations is not globally dependent on solar exposition, when it is not for air–sea surface fluxes. Fig. 1 shows global averaged air–sea surface fluxes as function of forecast lead-time. Averaged air–sea surface fluxes related to 24–36 h forecast are superimposed to the ones related to 0–12 h forecast; both originate from 00:00 UTC. Note that averaged fluxes for 0–12 and 24–36 h forecast are comparable in terms of duration and solar exposition. Surface solar radiation is minimal for 0–12 h when the solar exposition is maximum over the continents (Fig. 1a). Thermal radiation and sensible heat (Fig. 1b and d) remain almost constant whereas latent heat shows a constant rate of increase (Fig. 1c). Forecasts for both 0–12 and 24–36 h show similar solar radiation and dissimilar turbulent and thermal fluxes. These results show that (i) for short-range forecasts, solar radiation spin-up cannot be evaluated by forecast lead-times because the same period of the day must be considered; (ii) the spin-up signal for turbulent fluxes and thermal radiation are strongly smoothed in forecast lead-times analysis. This is a fundamental point for the methodology developed here. To illustrate this point, Table 2 gives the global Root Mean Square (RMS) of heat fluxes at $[\text{Time}] = 0$ and $[\text{Time}] = 12$ for different run durations. For each flux (latent, sensible and radiations), RMS decreases from $[\text{Step}] = 6$ to $[\text{Step}] = 24$ and increases slightly beyond. For $[\text{Step}] = 6$ and $[\text{Step}] = 12$, RMS is large due to geographical disparities of the solar warming. For $[\text{Step}] = 18$ and $[\text{Step}] = 24$, the run duration is greater than 12 h so that the averaged solar warming covers a larger extent of the globe and geographical disparities are reduced; the RMS decreases. RMS is the lowest for $[\text{Step}] = 24$, the length of the diurnal cycle. For larger run durations, geographical disparities are again present and RMS increases with a new diurnal cycle.

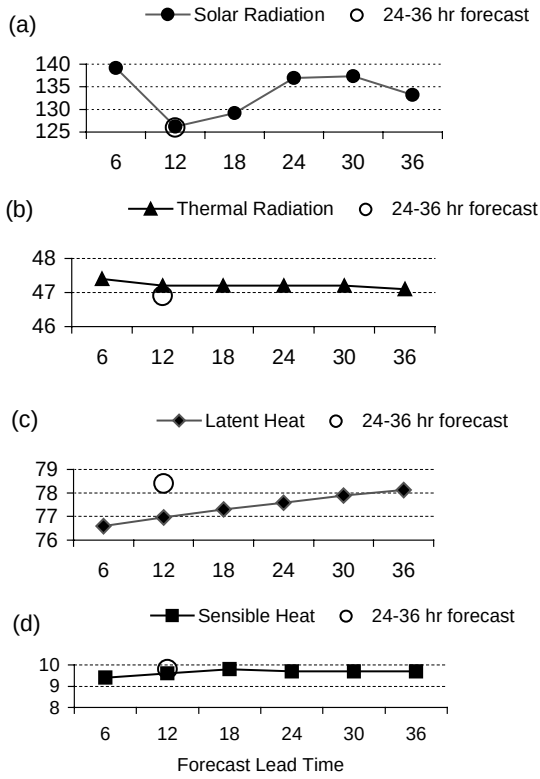

Fig. 1. Global averaged air–sea surface heat fluxes as a function of forecast-lead times for the period 1989–1991. Averaged fluxes related to 24–36 h forecast are superimposed to those related to 0–12 h forecast; both 24–36 and 0–12 h forecast originating from 00:00 UTC.

In order to compare fields corresponding to identical solar warming periods, a new nomenclature was introduced for specifying the difference between two forecast lead-times for the same initialization time. According to this nomenclature, the retained part of the difference is called *time-kept*, [Tk] and the common period *time-rejected*, [Tr]. The analysis is made for [Tk] constant, located by the central time of its time period. Fig. 2 illustrates some

Table 2
Global root mean square (Wm^{-2}) between heat fluxes estimated for [Time] = 00 and [Time] = 12 for several forecast lengths

Forecast length	Surface latent heat flux	Surface sensible heat flux	Surface solar radiation	Surface thermal radiation
6	19.89	19.04	301.11	5.10
12	14.19	14.33	202.32	3.49
18	5.74	7.51	97.10	2.03
24	1.08	0.44	2.12	0.52
30	4.07	3.84	60.14	1.15
36	4.75	4.81	65.51	1.24

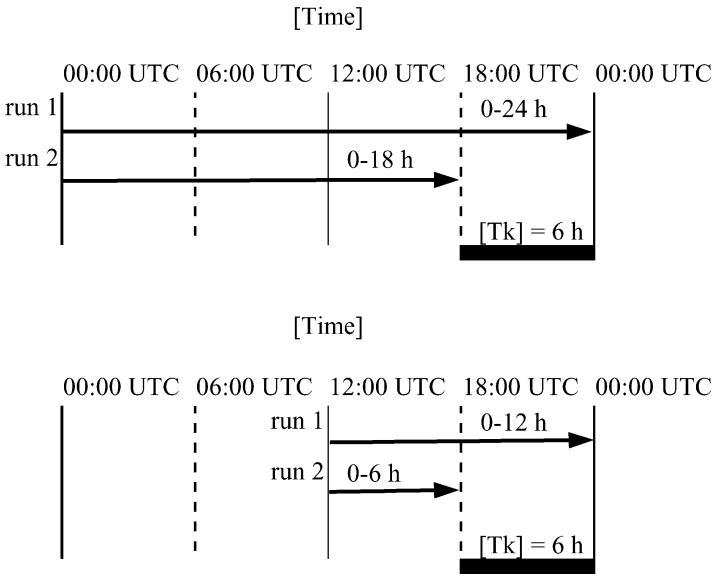

Fig. 2. A schematic illustration of averaged fluxes over the time period denoted as [Tk] (*time-kept*), and defined by the difference between two model runs in the form:

$$\left.\begin{array}{l}[\mathrm{Tk}] = \mathrm{run1} - \mathrm{run2},\\ [\mathrm{Tr}] = \mathrm{run2(time\text{-}rejected)}\end{array}\right\} \quad \text{for } [\mathrm{Time}] = \text{constant}$$

where [Time] is the initialization time. Both examples corresponds to the same central time of [Tk], equal to 21:00 UTC.

combinations between two forecast lead-times for $[\mathrm{Tk}] = 6$. Note that a forecast lead-time is characterized by $[\mathrm{Tr}] = 0$. With these conventions, averaged fluxes over [Tk] can be analyzed as a function of the range that it is from the initialization time, [Tr]. In addition, the spin-up may be defined by the difference between fields corresponding to $[\mathrm{Tr}] = 0$ and $[\mathrm{Tr}] \neq 0$, both located at the same central time of [Tk]. For example, $[\mathrm{Tk}] = 6$ located at 21 h for $[\mathrm{Tr}] = 6$ and $[\mathrm{Tr}] = 18$ corresponds, respectively, to 6–12 h forecast originating at 12:00 UTC and 18–24 h forecast originating at 00:00 UTC. This new nomenclature is unusual but it highlights the point because the main information is the change of air–sea surface fluxes as a function of the elapsed time from the initialization time.

3.2. Choice of the analysis period

Although ERA-40 covers more than 40 years, for comparison purposes with ERA-15, this study is restricted to those years covered by both ERA-40 and ERA-15, at the time that this study was undertaken. Thus, years 1989 to 1993 (inclusive) were considered. However, this period encloses the Mount Pinatubo eruption (July, 1991). The consequences of the Mount Pinatubo eruption over air–sea fluxes are not an easy matter, and a detailed analysis is beyond the scope of this study. Nevertheless, both ERA-40 and ERA-15 seasonal averaged fluxes were examined from 1989 to 1993 in order to ensure the consequences of the Mount

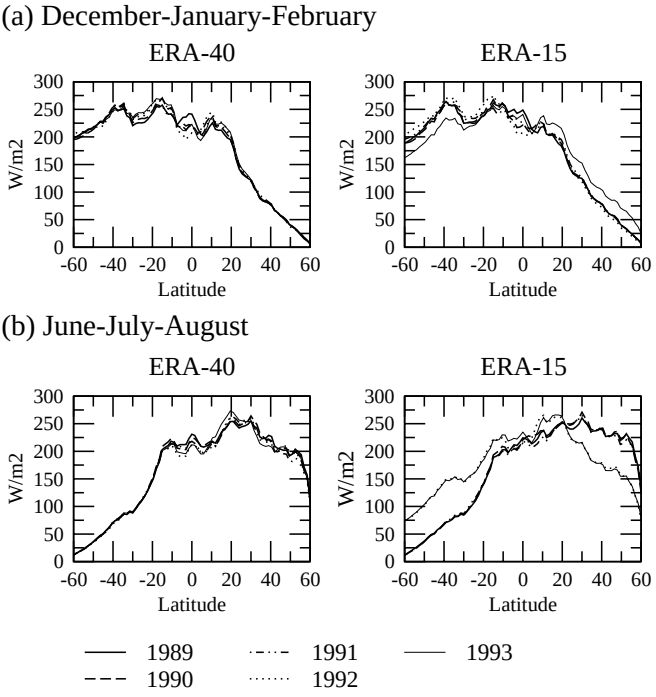

Fig. 3. Both ERA-40 and -15 meridional distribution of seasonal averaged solar radiation from 1989 to 1993: (a) December–January–February and (b) June–July–August.

Pinatubo eruption. The clearest impact of eruption on air–sea fluxes is shown by solar radiation (Fig. 3). ERA-40 zonal averaged solar radiation remain unchanged from 1989 to 1993 while significant changes were observed in ERA-15 from eight months after the Mount Pinatubo eruption (March-April-May, not shown). Changes in ERA-15 zonal averaged solar radiation can be seen by the setback of the curve related to both December-January-February 1993 (Fig. 3a) and June-July-August 1992–93 (Fig. 3b). It is difficult to identify the processes explaining the difference in behavior between ERA-40 and ERA-15. Nevertheless, it is probable that data assimilation system, which is the major point that distinguishes ERA-40 of ERA-15, is responsible for this difference. Indeed, assimilation techniques have a strong impact on the physical parameterizations response; on the other hand, radiation and convective schemes seem to be highly sensitive to the assimilated data. Under these conditions, this study of spin-up was newly set about for the period: 1989–91. Results show that qualitative conclusions remain unchanged but local spin-up of ERA-40 diminishes ($\approx 1\,\mathrm{W\,m^{-2}}$ of global averaged latent heat during JJA, not shown). These results confirm the robustness of the methodology and shows that it is not necessary to have many years to describe the model behavior. In addition, the assimilation of ERS-1 wave-height in ERA-40 from December 1991 to May 1993 generated erroneous wave fields especially in the tropics, which can affect air–sea fluxes. Consequently, to avoid these problems this study only considers the period 1989–91.

4. ERA-40 short-range forecasts spin-up

To constrain ocean models, oceanographers generally split the net surface heat flux into two components: net non-solar and solar fluxes. The non-solar component is the sum of turbulent (latent and sensible heat) and long-wave radiation fluxes. Long-wave and short wave radiative fluxes are the sum of upward and downward fluxes. Positive fluxes are oriented downwards. Non-solar flux spin-up fields are shown on Fig. 4, for [Tr] = 6 and [Tr] = 30 corresponding to June-July-August (JJA) and December-January-February (DJF) for the period 1989–91. Although the four fields generally range between $-20\,\mathrm{W\,m^{-2}}$ and $20\,\mathrm{W\,m^{-2}}$, extreme values of up to $80\,\mathrm{W\,m^{-2}}$ are observed with an increase of spin-up from [Tr] = 6 to [Tr] = 30. Note that during DJF (Fig. 4b), extremes of spin-up increase compared to JJA (Fig. 4a). During JJA, large spin-up is located in the southern hemisphere while during DJF the northern hemisphere is more concerned. Finally, from Fig. 4, it is concluded that (i) a significant spin-up affects both components of the net non-solar surface heat flux and (ii) this spin-up has a time trend and depends upon the season.

4.1. Large-scale features

On a global scale, Surface Latent Heat Flux (SLHF) spin-up increases with [Tr] and becomes nearly constant after 24 h regardless of the season (Fig. 5a). This means that beyond 24 h of model integration, SLHF are less influenced by the initialization procedure and have a better physical meaning. Nevertheless, this time of saturation is not uniform in space (Fig. 6a). The large-scale characteristics of spin-up displayed in Fig. 6 indicate that two areas can be distinguished: (i) a tropical band where the spin-up increases with [Tr] (the full line stays always above the dotted line) and (ii) north of 30°N and south of 30°S where a negative spin-up is observed. In tropical bands, spin-up stays constant after [Tr] = 24 and elsewhere the time of saturation is more or less equal to that of [Tr] = 6. Note that the time of stability found on a global scale (24 h) on Fig. 5a is the same as that in the tropics. Tropical regions have thus a major contribution to global spin-up behavior. Given that the same conclusion is obtained for several periods of the day, SLHF spin-up is quite independent of solar warming.

Regardless of the season, spin-ups of Surface Sensible Heat Flux (SSHF) centered on 09:00 UTC ([Tr] = 6, 18 and 30) are slightly different from those centered on 03:00 UTC ([Tr] = 12 and 24) (Fig. 5b). Conversely, to SLHF, this result indicates a slight dependence of SSHF spin-ups on solar warming. Spin-ups different from zero ([Tr] = 6, 18 and 30) show only a very weak tendency with [Tr] indicating that stability is reached as soon as [Tr] = 6. The meridional distribution of spin-up (Fig. 6b) identifies two distinct areas: (i) a band between 15°N and 20°S where spin-up occurs and (ii) areas beyond 20° north and south where negative spin-up occurs. Most areas have a non-monotone variation of spin-up with [Tr]. This behavior does not confirm the global result about the stability time of 6 h but rather indicates that there is a strong dispersion around the global spin-ups displayed in Fig. 5b.

Spin-up of Surface Solar Radiation (SSR) varies slightly with [Tr] (Figs. 5c and 6c) meaning that the stability time is nearly 6 h on global and large-scales. Note that on Fig. 6c, spin-up variations with [Tr] take into account several periods of the day affected by different

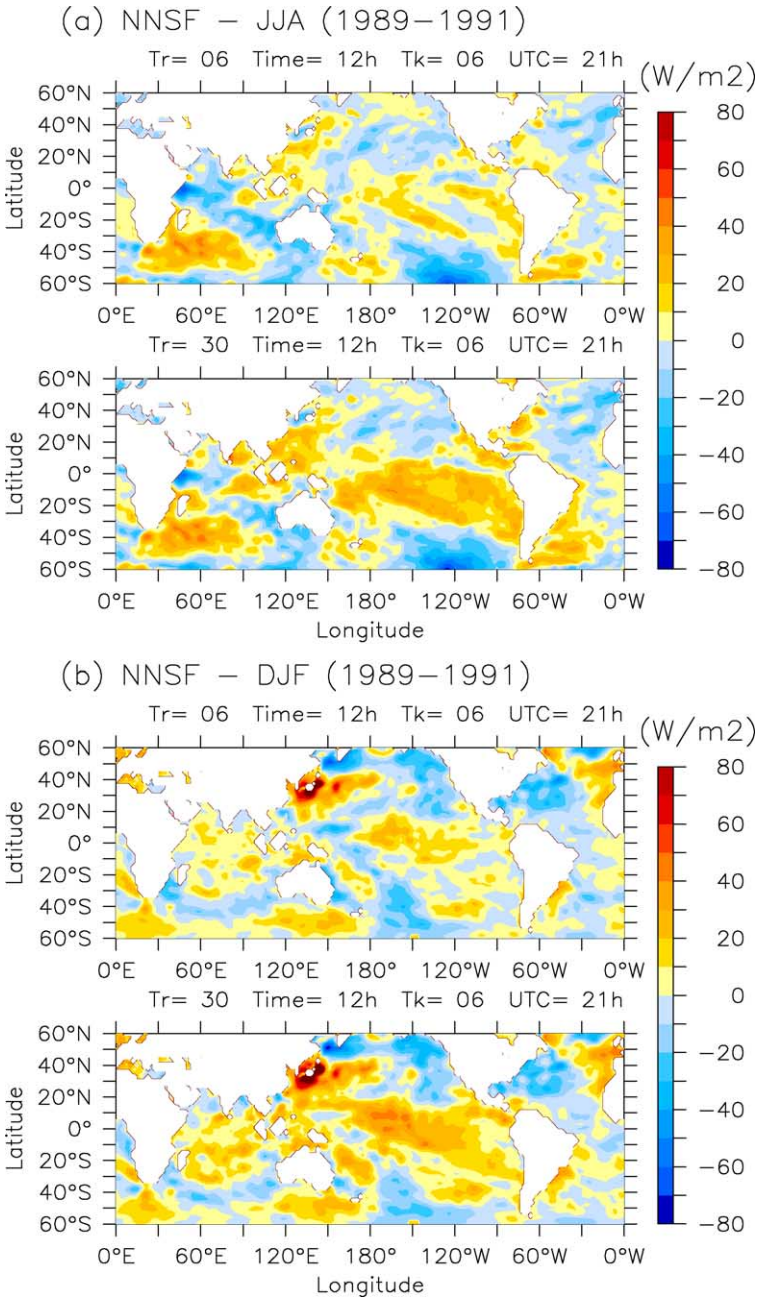

Fig. 4. Global distribution of seasonal averaged net non-solar flux spin-up for 1989–1991: (a) June–July–August and (b) December–January–February. Both figures (a) and (b) show spin-up for [Tr] = 6 and 30, respectively, from top to bottom.

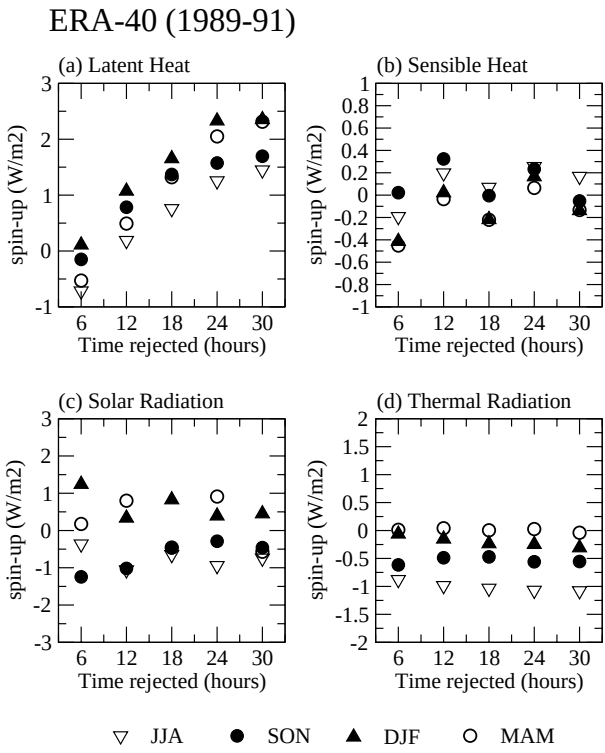

Fig. 5. Global averaged spin-ups of seasonal averaged air–sea surface heat fluxes for 1989–1991 as a function of [Tr] and for the four seasons. Representations of [Tr] = 6, 18, 30, 12 and 24 are centered on 09:00 and 03:00 UTC, respectively.

solar warming periods. In spite of this, spin-up remains almost constant with time. Global averaged Surface Thermal Radiation (STR) has a generally constant negative spin-up and no spin-up during SON (Fig. 5d). On a large-scale (Fig. 6d), negative spin-up occurs beyond 30° north and south; spin-ups remain almost similar especially beyond [Tr] = 18.

In terms of percentages, radiative flux spin-ups are smaller than those of turbulent flux but both sensible heat and radiative fluxes have spin-ups with the same order of magnitude; latent heat showing largest spin-up. Under this condition, all flux spin-ups can be considered affecting net surface heat budget. However, because on large-scale the stability time of radiative flux spin-ups are generally the same, hereafter spin-up study will focus solely on the turbulent heat fluxes.

4.2. Regional scale features

Section 4.1 was devoted to describing large-scale characteristics of spin-up. This section aims to analyze spin-up of the turbulent heat fluxes on regional scales. Four regions were selected: Boreal East Atlantic (0°–40°W; 30°–60°N), the Gulf Stream (40°–80°W;

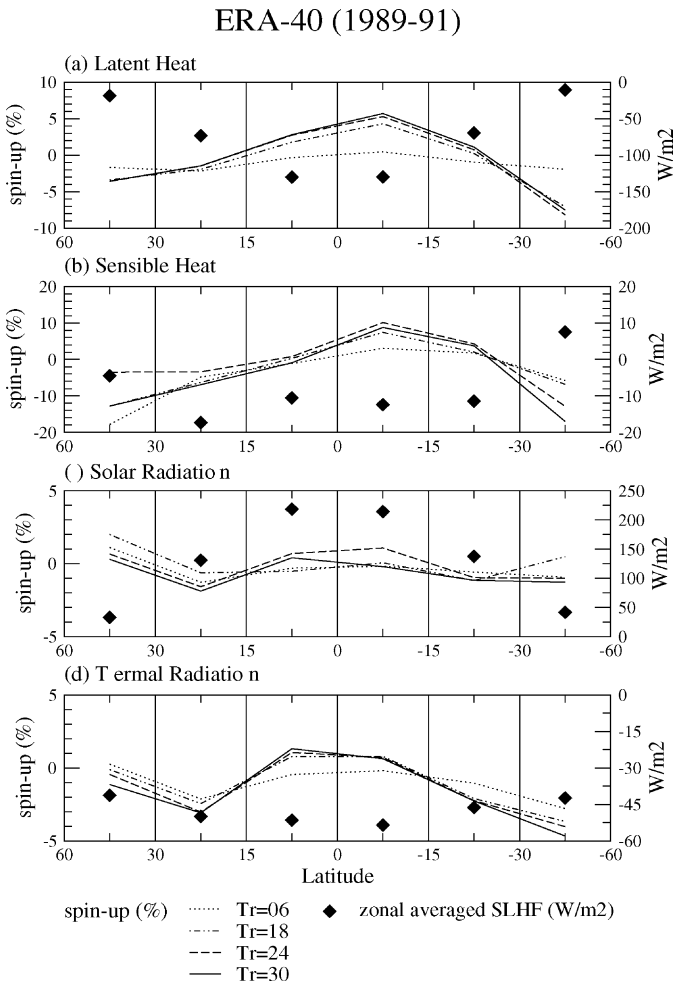

Fig. 6. Meridional distribution of air–sea surface heat fluxes spin-ups for 1989–91 corresponding to [Tr] = 6, 18, 24 and 30. Spin-ups related to [Tr] = 6 and 30 are centered on 09:00 UTC whereas those related to [Tr] = 18 and 24 are centered on 21:00 and 06:00 UTC, respectively. Across the Tropics, spin-ups are computed over bands of 15° of latitude wide whereas beyond 30° north and south spin-ups are computed over bands of 30° of latitude wide. Zonal averaged fluxes for 0–6 h forecast computed from 06:00 UTC (centered on 09:00 UTC) are superimposed to spin-up representation.

30°–60°N), Kuroshio (120°–160°E; 20°–50°N), and the Tropical Pacific (80°W–160°E; 0°–30°S). The Boreal East Atlantic was selected as an example of weak spatial variability of fluxes; the Gulf Stream and Kuroshio for strong intensity and spatial variability of surface heat exchanges; and the Tropical Pacific for the coupled air–sea event ENSO (El Niño-Southern Oscillation).

Spin-ups on regional-scale (Fig. 7) are quite different from those on large-scales (Fig. 6), especially for SSHF. SLHF spin-ups never exceed 15% but SSHF spin-ups can be larger

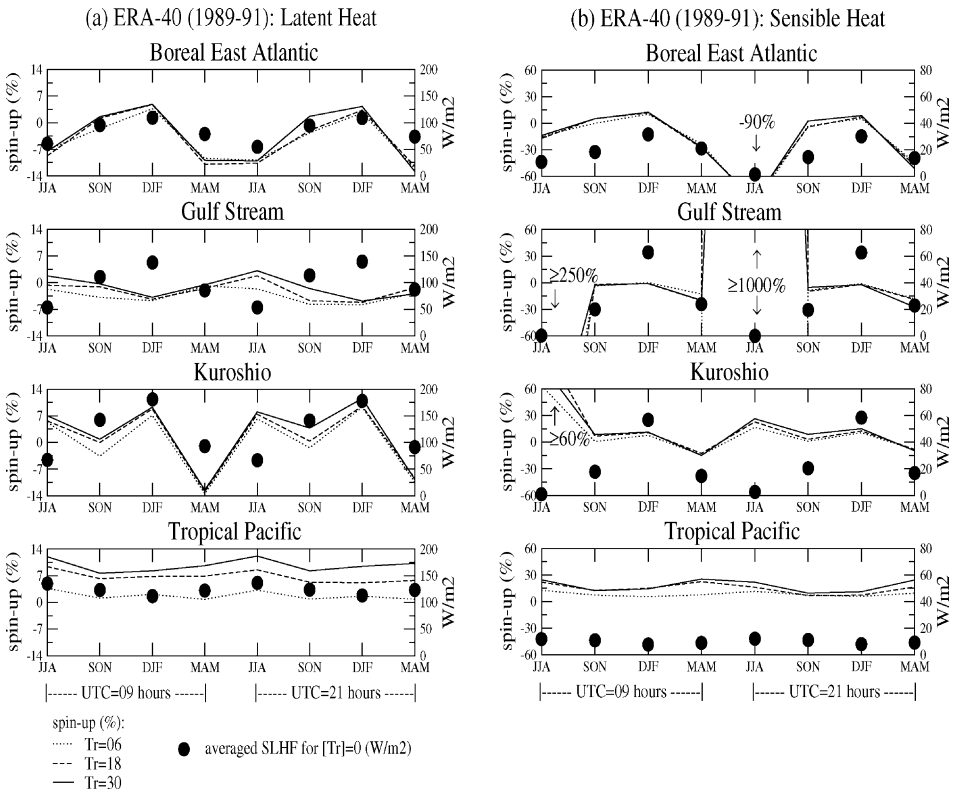

Fig. 7. Spin-ups of regional averaged (a) latent and (b) sensible heat fluxes as a function of the four seasons. Both figures (a) and (b) shows Boreal East Atlantic, Gulf Stream, Kuroshio, and Tropical Pacific, respectively, from top to bottom. Lines represent spin-ups related to [Tr] = 6, 18 and 30 and circles averaged fluxes for 0–6 h forecast ([Tr] = 0). Spin-ups related to [Tr] = 6, 18 and 30 are represented for two periods of the day: 09:00 and 21:00 UTC corresponding, respectively, to night and day on Tropical Pacific.

than 60% in Boreal East, Gulf Stream and Kuroshio. This is because SSHF intensities are much smaller (close to zero) than those of SLHF are. Fig. 7 shows that turbulent flux spin-ups depend on the season meaning that it could be associated with weather regimes.

In the Boreal East Atlantic, Gulf Stream and Kuroshio, SLHF and SSHF spin-ups gen-

Fig. 8. Diurnal cycle of regional averaged (a) latent and (b) sensible heat fluxes computed for 1989–1991 as follows: [Tr] = 0 corresponding to 0–6 h forecast from 00:00, 06:00, 12:00, 18:00 UTC (black diamond); [Tr] = 6, 12, 18 and 24, corresponding to, respectively, 0–6, 6–12, 12–18 and 18–24 h forecasts from 00:00 UTC (gray diamond); [Tr] = 6, 12, 18 and 24, corresponding to, respectively, 0–6, 6–12, 12–18 and 18–24 h forecasts from 12:00 UTC (white diamond). Both figures (a) and (b) shows June–July–August and December–January–February, respectively, from left to right and Boreal East Atlantic, Gulf Stream, Kuroshio, and Tropical Pacific, respectively, from top to bottom. Diurnal cycle corresponding to [Tr] = 0 is displayed twice (one following the other) because those obtained from 12:00 UTC reaches into the next day. Fluxes are plotted at the central time of cumulated interval ([Tk] = 6) at 03:00, 09:00, 15:00 UTC and so on. Spin-ups can be directly obtained by the gap between flux corresponding to successive [Tr] and the run [Tr] = 0.

(a) Latent Heat

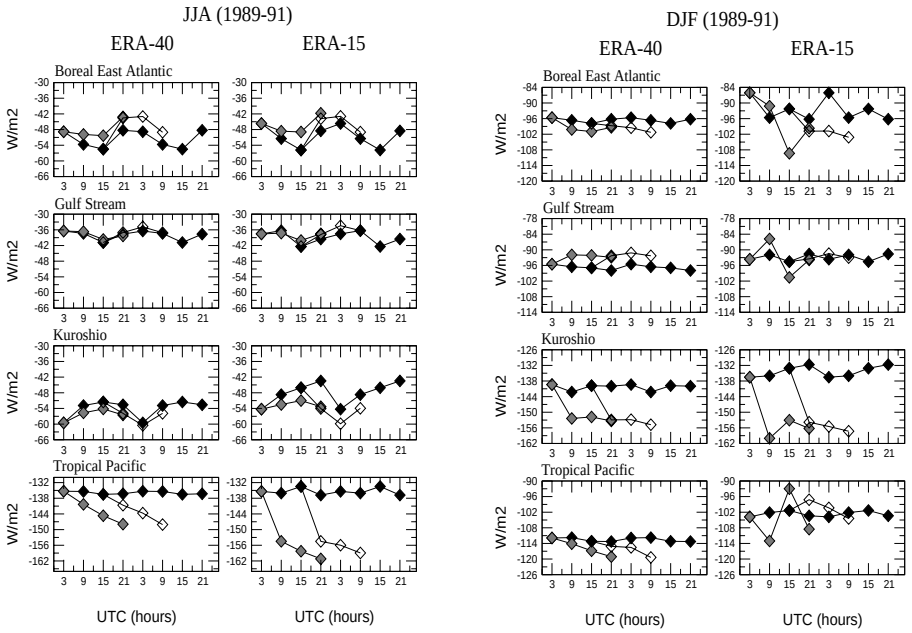

(b) Sensible Heat

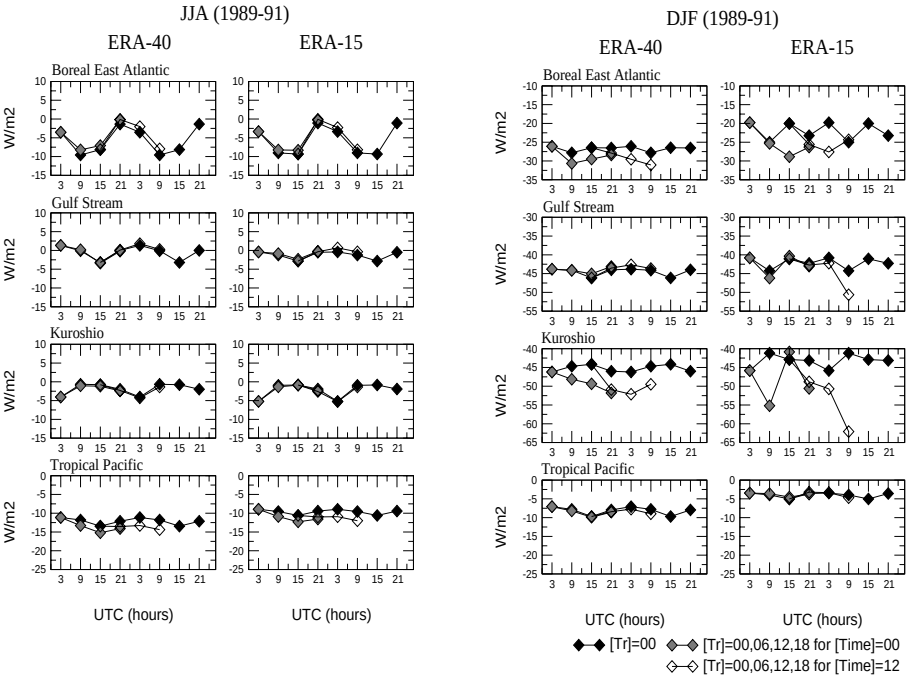

erally stabilize as early as [Tr] = 6. In the Tropical Pacific, SLHF spin-ups for [Tr] = 18 are generally close to those for [Tr] = 30. This result confirms the mainly contribution of tropical region on the global stability time of 24 h regardless of the season. SSHF in Tropical Pacific shows a stability time of spin-up varying with the seasons and ranging from [Tr] = 6 in autumn to [Tr] = 18 in spring.

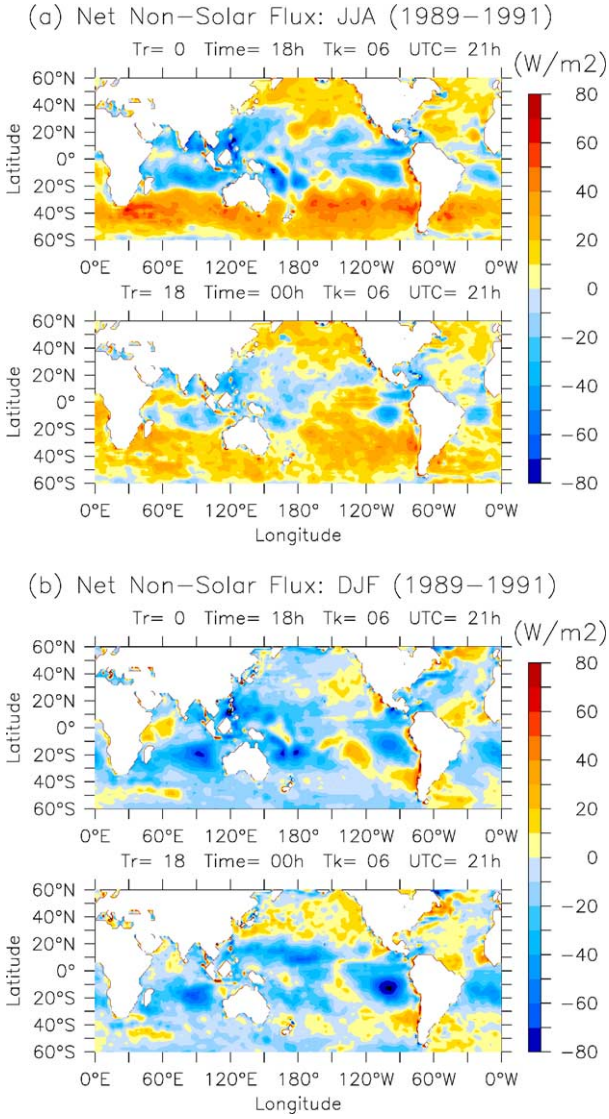

Fig. 9. Global distribution of biases between both ERA-40 and -15 net non-solar flux for 1989–1991: (a) June–July–August and (b) December–January–February. Both figures (a) and (b) show biases for [Tr] = 0 and 18, respectively, from top to bottom.

To conclude this section, regional results confirm those obtained on global and large-scales but some seasonal disparities have to be taken into account on the regional scales.

5. ERA-40 and ERA-15 intercomparison

In this section, ERA-40 and ERA-15 turbulent heat fluxes are compared in the four selected regions. The strategy adopted was firstly to compute fluxes from initialization times 00:00, 06:00, 12:00, 18:00 UTC for [Tr] = 0 h. and secondly to compute fluxes from initialization times 00:00 and 12:00 UTC for [Tr] = 0, 6, 12, 18 h. Thus, for a given initialization time, the successive [Tr] give access to the temporal trend of the fluxes. Moreover, spin-ups can be directly obtained by the gap between the flux corresponding to successive [Tr] and the run [Tr] = 0 (Fig. 8).

In most regions, ERA-15 spin-ups are greater than those of ERA-40 are, especially in DJF. A good illustration is also given by SLHF in Tropical Region in JJA. Note that, ERA-40 spin-ups always stabilize whereas those of ERA-15 are mainly chaotic. This behavior is especially highlighted in Boreal East Atlantic and Kuroshio in DJF. With the objective to force ocean models as accurately as possible, it is very important to use fluxes with the shortest spin-up. From this point of view, ERA-40 would give better results than ERA-15.

ERA-40 net non-solar flux are compared to those of ERA-15 for [Tr] = 0 and [Tr] = 18 in JJA (Fig. 9a) and in DJF (Fig. 9b). These fields clearly indicate the magnitude of biases between the two reanalysis. Biases about 30 W m^{-2} and locally up to 50 W m^{-2} are observed for [Tr] = 0 and south of 20°S (Fig. 9a). Generally, biases are weaker for [Tr] = 18 than for [Tr] = 0. This result confirms the convergence of both ERA-40 and ERA-15 numerical simulations when it moves away from the initialization time. This is because both models have similar physical packages. Nevertheless, even for [Tr] = 18 the bias remains high (40 W m^{-2}) in some regions. In terms of oceanographic predictability, we think this is significant because small bias (for instance 20 W m^{-2}) in the net surface heat flux can induce significant errors in the mixed layer parameters (Kelly and Qiu, 1995).

6. Summary and conclusions

The main objective of this paper was to quantify short-range forecast spin-ups of air–sea surface heat fluxes in the 40-year ECMWF re-analysis. This evaluation was carried out for the period 1989–1991. Spin-up was evaluated for each component of the heat flux on global, large-scale (over bands of latitudes) and regional scales. Impacts of seasonal cycle on spin-up were also considered. Finally, a comparison of ERA-40 with -15 was performed.

Radiative fluxes spin-ups were found to be weaker than 5% with a time of stability generally approximating 6 h for all scales. Conversely, turbulent heat flux spin-ups and its time of stability were found to be much greater than those of radiative fluxes. On a global scale, latent heat flux spin-up levels off after 24 h. Analysis on large-scales showed that this behavior is due to a major contribution of tropical latitudes. Beyond 30° north and south, spin-up had stabilized by around 6 h. Sensible heat flux spin-up stabilized as soon as 6 h on a global scale but on large-scale a strong dispersion is founded around the global value.

Finally, the regional analysis confirmed the global and large-scales results though some seasonal modulations appear on turbulent flux spin-ups and their stability-time.

Intercomparison between ERA-40 and -15 showed that ERA-40 spin-ups are in most cases weaker than in ERA-15 and always stabilize, whereas those in ERA-15 are largely chaotic. In terms of oceanic mixed layer predictability, these two points are crucial. That is the reason why ERA-40 surface heat fluxes give a real added value in comparison with ERA-15. The basis of these results may be caused by the use of non-representative 10-m wind observations from isolated islands (Beljaars and Kållberg, 2001; Kållberg, 1997). Another cause could be the different data assimilation techniques used. ERA-15 uses an optimal interpolation technique, which assimilates data without any physical constraint. Consequently, initial movement and mass fields are strongly unbalanced in the sense of the model's equations; this noise induces strong and chaotic surface flux spin-ups. Conversely, ERA-40 uses a 3D variational assimilation technique, which assimilates data under physical constraints given by the model. Consequently, turbulent surface fluxes have limited spin-ups and monotonic temporal evolutions.

The choice of surface fluxes produced by atmospheric models is often an underestimated question. Our results suggest that this question is important when the proposal is to compare model-to-model or in situ data to model outputs. This question also arises when the purpose is to constrain ocean models. For instance, Bonekamp et al. (1999) have shown that solely thermodynamic forcing is able to trigger the ocean Antarctic Circumpolar Wave mode. Finally, in support of oceanographic interests, the same work should be extended to surface momentum fluxes and the consequence of air–sea surface fluxes spin-up analyzed by running a global ocean model.

Acknowledgements

The authors would express their appreciation to Professor M.T. Montgomery for several comments that have improved the clarity of the presentation and also thank anonymous reviewers for improving the manuscript. This work has been funded by the European Union Framework V project ERA-40 (EVK2-CT-1999-00027). The authors would like to thank Pascal Simon, Météo-France's Coordinator of ERA-40, who supported this study.

References

Arpe, K., & Stendel, M., 1996. Evaluation of the ECMWF re-analysis with emphasis on the precipitation. In: Proceedings of the 20th Climate Diagnostic Workshop. Seattle, Washington, USA, 23–27 October 1995, pp. 152–155.

Beljaars, A.C.M., 1995. The parameterization of surface fluxes in large-scale models under free convection. Quart. J. Roy. Meteor. Soc. 121, 255–270.

Beljaars, A.C.M., 1997. Air–sea interaction in the ECMWF model. In: Proceedings of the Seminar on Atmosphere–Surface Interaction. ECMWF, Reading, 8–12 September 1997, pp. 33–52.

Beljaars, A., Kållberg, P., 2001. Ocean fluxes in the ECMWF 40-year re-analysis (ERA-40). In: Proceedings of the WCRP/SCOR Workshop on Intercomparison and Validation of Ocean-Atmosphere Flux Fields. WCRP-115, WMO/TD-No 1083. Bolger Center, Potomac, MD, USA, 21–24 May 2001, pp. 18–20.

Bengtsson, L., Shukla, J., 1988. Integration of space and in situ observations to study global climate change. Bull. Am. Meteorol. Soc. 69 (10), 1130–1143.

Courtier, P., Anderson, E., Heckley, W., Pailleux, J., Vasiljevic, D., Hamrud, M., Hollingsworth, A., Rabier, F., Fisher, M., 1998. The ECMWF implementation of the three-dimensional variational assimilation (3D-Var). Part 1. Formulation. Quart. J. Roy. Met. Soc. 124, 1783–1867.

Bonekamp, H., Sterl, A., Komen, G.J., 1999. Interannual variability in the Southern Ocean from an ocean model forced by European Centre for Medium-Range Weather Forecasts reanalysis fluxes. J. Geophys. Res. 104 (C6), 13317–13331.

Giordani, H., Planton, S., 2000. Modeling and analysis of ageostrophic circulation over the Azores Oceanic Front during the SEMAPHORE Experiment. Monthly Weather Rev. 128 (7), 2270–2287.

Gibson, J.K., Kållberg, P., Uppala, S., Hernadez, A., Nomura, A., Serrano, E, 1999. ECMWF Re-Analysis Project Report Series No 1. ERA-15 Description, Version 2, January 1999, 73 pp.

Hagemann, S., Arpe, K., Bengtsson, L., Kirchner, I., 2002. Validation of precipitation from ERA-40 and an ECHAM-4.5 simulation nudged with ERA-40 data. 3. Workshop on Re-analysis. ECMWF, Shinfield Park, Reading, UK, 5–9 November 2001, pp. 211–227.

Janssen, P.A.E.M., Doyle, J.D., Hansen, B., Isaksen, L., Viterbo, P., 1997. The impact of ocean waves on the atmosphere. In: Proceedings on Atmosphere–Surface Interaction. ECMWF Seminar, Reading, UK, 8–12 September 1997, pp. 85–111.

Kållberg, P., 1997. Aspects of the Re-analysed Climate. ECMWF Re-Analysis Project Report Series No 2. ECMWF, Reading, UK, 89 pp.

Kelly, G., Li, X., 2002. Assimilation TOVS/VTPR/SSMI Radiances and use of Australian surface PAOBs. ERA-40 Project Report Series, 3. Workshop on Re-analysis. ECMWF, Shinfield Park, Reading, UK, 5–9 November 2001, pp. 123–148.

Kelly, K.A., Qiu, B., 1995. Heat flux estimates for the Western North Atlantic. Part I. Assimilation of Satellite Data into a Mixed Layer Model. J. Phys. Oceanogr. 25 (10), 2344–2360.

Kistler, R., Kalnay, E., Collins, W., Saha, S., White, G., Woollen, J., Chelliah, M., Ebisuzaki, W., Kanamitsu, M., Kousky, V., van den Dool, H., Jenne, R., Fiorino, M., 2001. The NCEP-NCAR 50-year re-analysis. Monthly means CD-ROM and documentation. Bull. Am. Meteorol. Soc. 82 (2), 247–268.

Lorenc, A.C., 1981. A global three-dimensional multivariate statistical interpolation scheme. Monthly Weather Rev. 109 (4), 701–721.

Nomura, A., 1997. Global Sea Ice Concentration Data Set for use with the ECMWF Re-Analysis System. ECMWF Project Report Series 4. Previously Issued as ECMWF Technical Report No. 76. March 1995.

Rayner, N.A., Parker, D.E., Horton, E.B., Folland, C.K., Alexander, L.V., Rowell, D.P., Kent, E.C., Kaplan, A., 2002. Global analyses of SST, sea ice and night marine air temperature since the late 19th century. J. Geophys. Res., in press.

Schubert, S.D., Rood, R.B., Pfaendtner, J., 1993. An assimilated dataset for earth science applications. Bull. Am. Meteorol. Soc. 74 (12), 2331–2342.

Simmons, A.J., Gibson, J.K., 2000. The ERA-40 Project Plan. ERA-40 Project Report Series 1. ECMWF, Shinfield Park, Reading, UK.

Trenberth, K.E., Olson, J.G., 1988. An evaluation and intercomparison of global analyses from the national meteorological center and the European centre for medium range weather forecasts. Bull. Am. Meteorol. Soc. 69 (9), 1047–1056.

White, G., Saha, S., 1999. Estimation of the global energy and water cycle from global data assimilation. In: Browning, K.A., Gurney, R.J. (Eds.), Global Energy and Water Cycles. Cambridge University Press, Cambridge, UK, pp. 55–60.

Uppala, S., Gibson, J.K., Fiorino, M., Hernandez, A., Kållberg, P., Xu, L., Onogi, K., Saarinen, S., 2000. In: Proceedings of the Second WCRP International Conference on Re-analyses. WCRP-109, WMO/TD-No 985. Wokefield Park, Reading, UK, 23–27 August 1999, pp. 9–13.